EARTHQUAKE ENGINEERING AND STRUCTURAL DYNAMICS
Earthquake Engng Struct. Dyn. 2002; **31**:833–850 (DOI: 10.1002/eqe.126)

Displacement-based seismic analysis for out-of-plane bending of unreinforced masonry walls

K. Doherty[1], M. C. Griffith[1,*,†], N. Lam[2] and J. Wilson[2]

[1] *Department of Civil and Environmental Engineering, Adelaide University, Adelaide, SA 5005, Australia*
[2] *Department of Civil and Environmental Engineering, University of Melbourne, Victoria 3010, Australia*

SUMMARY

This paper addresses the problem of assessing the seismic resistance of brick masonry walls subject to out-of-plane bending. A simplified linearized displacement-based procedure is presented along with recommendations for the selection of an appropriate substitute structure in order to provide the most representative analytical results. A trilinear relationship is used to characterize the real nonlinear force–displacement relationship for unreinforced brick masonry walls. Predictions of the magnitude of support motion required to cause flexural failure of masonry walls using the linearized displacement-based procedure and quasi-static analysis procedures are compared with the results of experiments and non-linear time-history analyses. The displacement-based procedure is shown to give significantly better predictions than the force-based method. Copyright © 2002 John Wiley & Sons, Ltd.

KEY WORDS: masonry; strength; displacement; bending; seismic; assessment

1. INTRODUCTION

In recent years, displacement-based (DB) design philosophies have gained popularity for the seismic design and evaluation of ductile structures, e.g. References [1–3]. However, designers perceive unreinforced masonry (URM) to possess very limited ductility so that its seismic performance has been considered to be particularly sensitive to peak ground accelerations [4]. Consequently, elastic design methods as opposed to DB design philosophies have been thought applicable. In contrast, recent research has shown that dynamically loaded URM walls can often sustain accelerations well in excess of their 'quasi-static' capabilities [5–7]. This dynamic 'reserve capacity' to displace out-of-plane without overturning arises because the wall's 'post-cracking' dynamic response is generally governed by stability mechanisms.

* Correspondence to: M. C. Griffith, Department of Civil and Environmental Engineering, Adelaide University, Adelaide, SA 5005, Australia.
† E-mail: mcgrif@civeng.adelaide.edu.au

Contract/grant sponsor: Australian Research Council; contract/grant number: A89702060.

Received 16 November 2000
Revised 29 May 2001
Accepted 17 July 2001

That is to say, geometric instability of a URM wall will only occur when the mid-height displacement exceeds its stability limit [8]. Indeed, research into face loaded infill masonry panels by Abrams has shown that under dynamic loading, one of the key responses governing wall stability is the size of the maximum displacement [9]. This suggests that DB design philosophies could provide a more rational means of determining seismic design actions for URM walls in preference to the traditional 'quasi-static' force-based approach presently in use.

Currently available static and dynamic predictive models have not been able to account for the large displacement post-cracking behaviour and 'reserve capacity' of URM walls when subjected to the transient characteristics of real earthquake excitations. Traditional 'quasi-static' approaches are restricted to considerations taken at a critical 'snapshot' in time during the response and hence the actual time-dependent characteristics are not modelled. As a result, the 'reserve capacity' to rock is not recognized, thereby providing a conservative prediction of dynamic lateral capacity. While such procedures may result in a reasonable design for new structures, they may be too conservative for the seismic assessment of existing URM structures where unacceptable economic penalty could be imposed if 'reserve capacity' is ignored. In recognition of this problem, a velocity-based approach founded on the equal-energy 'observation' was developed [10], which considers the energy balance of the responding wall. The main disadvantage of this procedure is that the energy demand calculation is very sensitive to the selection of elastic natural frequency and is only relevant for a narrow band of frequencies. Clearly, there is a need for the development of a rational and simple analysis procedure, encompassing the essence of the dynamic rocking behaviour and thus accounting for the reserve capacity of the URM wall.

A major outcome of the collaborative analytical and experimental research carried out at the Universities of Adelaide and Melbourne has been the development of a rational analysis procedure which models the reserve capacity of the rocking wall. This procedure is based on a linearized displacement-based (DB) approach and has been adapted for a wide variety of URM wall boundary conditions.

The structure of this paper is as follows: A single-degree-of-freedom idealization of the rocking behaviour of URM walls based on their force–displacement (F–Δ) relationships is described in detail in Section 2. This idealization applies to URM walls, such as parapet walls and non-loadbearing (or lightly loaded) simply supported walls (i.e. possessing different boundary conditions). The F–Δ relationships have been developed in Section 3 for URM walls behaving as rigid blocks which rock about pivot points at the fully cracked sections. In Section 4, this idealization is relaxed by including axial and flexural deformations for walls subjected to high axial pre-compression. The sections of the wall where this deformation is included are referred to as 'semi-rigid' blocks. In Section 5, the substitute structure concept is applied to further simplify the single-degree-of-freedom (SDOF) models so the response behaviour of URM walls can be predicted using displacement response spectra. The DB procedure has been verified by comparing the predicted dynamic lateral capacities of simply supported URM walls with a series of non-linear time history analyses (THA).

2. SINGLE-DEGREE-OF-FREEDOM IDEALIZATION OF URM WALLS

A cracked URM wall rocking with large horizontal displacements may be modelled as rigid blocks separated by fully cracked cross-sections. This assumption is realistic provided that

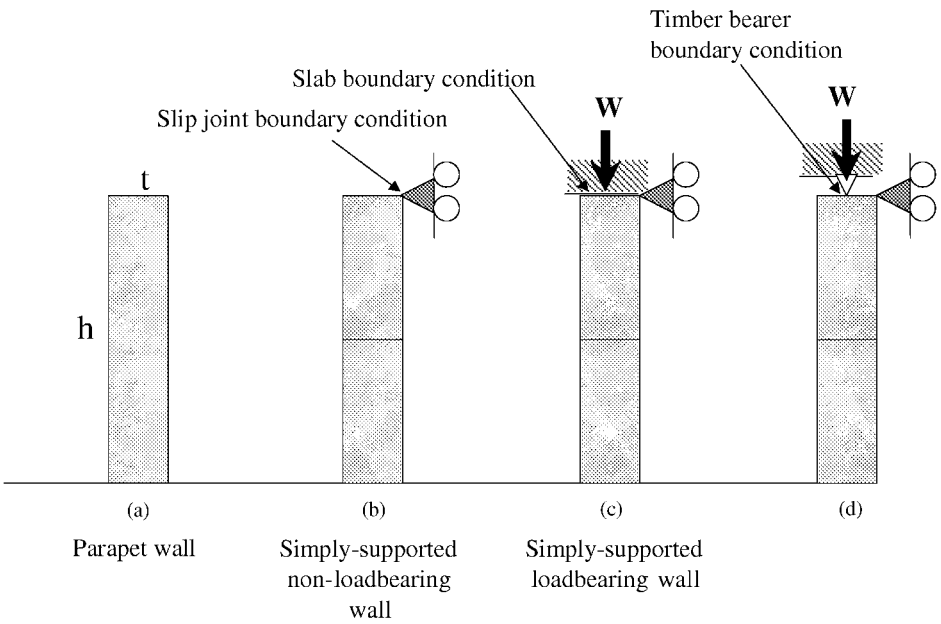

Figure 1. Unreinforced masonry wall support configurations.

there is little, or no, vertical pre-compression to deform the blocks. The class of URM walls satisfying such conditions include cantilever walls (parapet walls) and simply supported walls which span vertically between supports at ceiling and floor levels as shown in Figures 1(a)–1(d) where the support motions can reasonably be assumed to move simultaneously. The case of differential support motion such as might occur in buildings with 'flexible' floor diaphragms [11] are also important but beyond the scope of this paper. The SDOF idealization of these URM walls may be modelled using the displacement profile of a rocking wall (in a fashion similar to the SDOF idealization of a multi-storey building based on the fundamental modal deflection).

From standard modal analysis principles, the equation of motion governing the rocking behaviour of the cracked URM wall is very similar to the equation of motion governing the response behaviour of the simple lumped mass SDOF model shown in Figure 2. Thus, the mass of the system models the overall inertia force developed in the wall, whilst the spring models the ability of the wall to return to its vertical position during rocking by virtue of its self-weight. Provided that the inertia force developed in the lumped mass and the restoring force developed in the spring are in the correct proportion, the displacement of the lumped mass SDOF system and the wall system will always be proportional to each other. Consequently, the response of these two systems can be related by a constant factor at any point in time during the entire time-history of the rocking response. It can be shown that the correct proportion is achieved if the lumped mass is equated to the effective modal mass of the wall (calculated in accordance with the displacement profile during rocking) and the restoring force is equated to the base shear (or total horizontal reaction) of the wall.

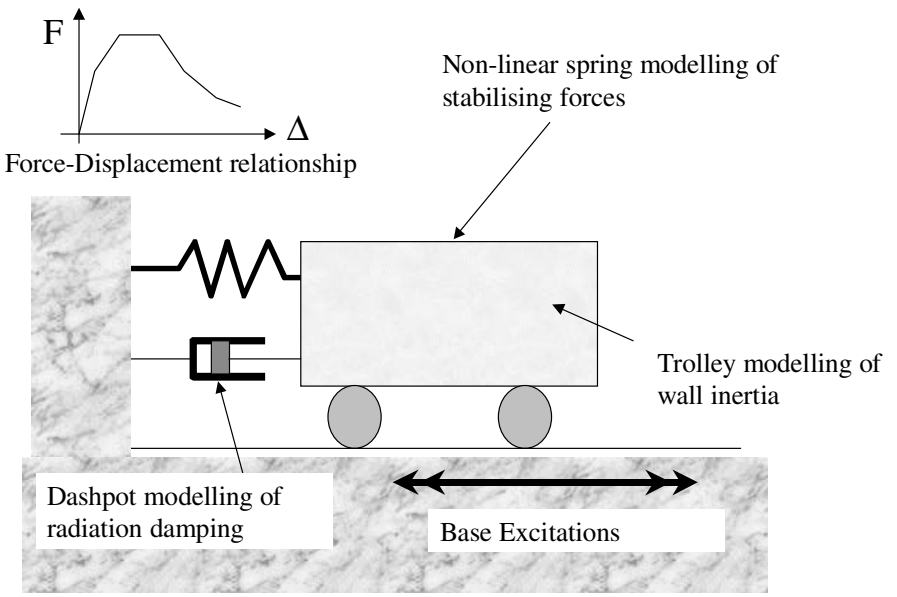

Figure 2. Idealized non-linear single-degree-of-freedom model.

The computed displacement, velocity and acceleration of the lumped mass are defined as the effective displacement, velocity and acceleration, respectively.

The equation of motion of the lumped mass SDOF system can, therefore, be expressed as follows:

$$M_e a_e(t) + C v_e(t) + F(\Delta_e(t)) = -M_e a_g(t) \tag{1}$$

where $a_e(t)$ is the effective acceleration, $a_g(t)$ the acceleration at wall supports, $v_e(t)$ the effective velocity, $\Delta_e(t)$ the effective displacement, C the viscous damping coefficient and $F(\Delta_e(t))$ the non-linear spring force which can be expressed as a function of $\Delta_e(t)$ (NB: $F(\Delta_e(t))$ is abbreviated hereafter as $F(\Delta_e)$).

The effective modal mass (M_e) is calculated by dividing the wall into a number of finite elements each with mass (m_i) and displacement (δ_i) and applying Equation (2) which is defined as follows:

$$M_e = \frac{(\sum_{i=1}^{n} m_i \delta_i)^2}{\sum_{i=1}^{n} m_i \delta_i^2} \tag{2}$$

For a wall with uniformly distributed mass, the effective mass for both parapet walls and walls simply supported at their top and bottom has been calculated to be three-fourths of the total mass, based on standard integration techniques. Thus,

$$M_e = 3/4M \tag{3}$$

where M is the total mass of the wall.

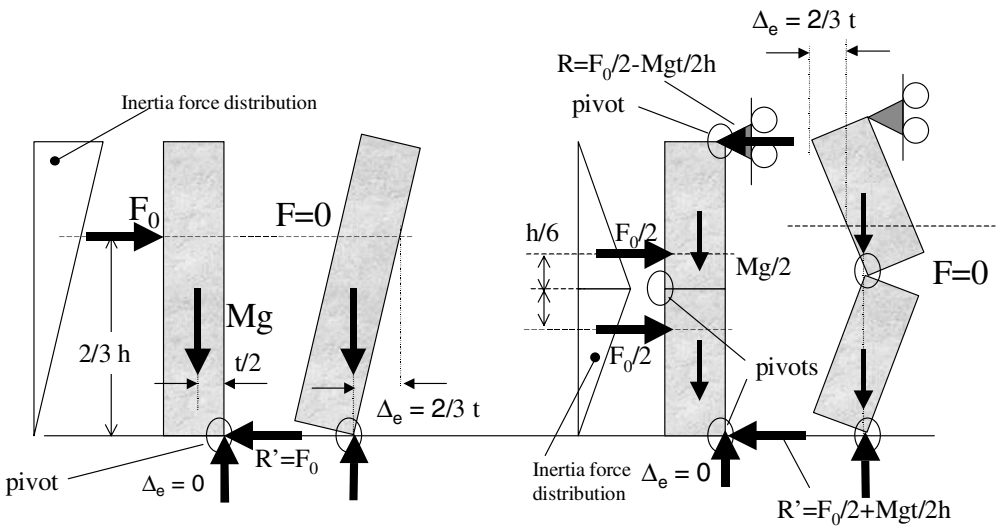

Figure 3. Inertia forces and reactions on rigid URM walls.

A similar expression, Equation (4), also derived using standard modal analysis procedures, is used to define the effective displacement (Δ_e).

$$\Delta_e = \frac{\sum_{i=1}^{n} m_i \delta_i^2}{\sum_{i=1}^{n} m_i \delta_i} \tag{4}$$

It can be shown from Equation (4) that

$$\Delta_e = 2/3\Delta_t \text{ (for a parapet wall) and} \tag{5a}$$

$$\Delta_e = 2/3\Delta_m \text{ (for simply-supported wall)} \tag{5b}$$

where Δ_t and Δ_m are the top of wall and mid-height wall displacements, respectively.

Note that both Equations (3) and (5) are based on the assumption of a triangular-shaped relative displacement profile. This can be justified for a rocking wall where the displacements due to rocking far exceed the imposed support displacements. The accuracy of this assumption has been verified with shaking table tests and THA as described in Reference [12]. Thus, the resultant inertia force is applied at two-thirds of the height of a parapet wall, and one-third of the upper half of the simply supported wall measured from its mid-point (Figures 3(a) and 3(b)).

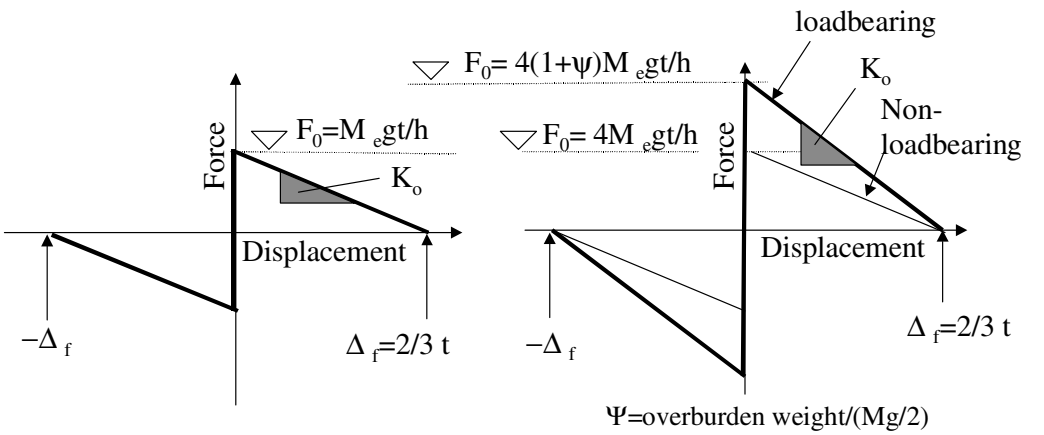

Figure 4. Force–displacement relationships of rigid URM walls.

3. MODELLING OF CRACKED UNREINFORCED MASONRY WALLS AS RIGID BLOCKS

The spring force function $F(\Delta_e)$ can be obtained by determining the total horizontal reaction (or base shear) at different displacements using basic principles of static equilibrium. For example, the overturning equilibrium of a parapet wall about the pivot point at the base of the wall can be used to determine $F(\Delta_e)$.

For a parapet wall at the point of incipient rocking (i.e. $\Delta_e = 0^+$ or alternatively $\Delta_t = 0^+$), moment equilibrium leads to (refer Figure 3(a)) the expression:

$$Mgt/2 = F_0(2/3)h \tag{6a}$$

Solving for F_0 (F at $\Delta_e = 0^+$) and substituting Equation (3) into Equation (6a) gives

$$F_0 = M_e(gt/h) \tag{6b}$$

For a parapet wall at the point of instability ($\Delta_e = 2/3t$ or alternatively $\Delta_t = t$), the force F required for static equilibrium of the wall is given by

$$F = 0 \tag{6c}$$

Therefore, the $F(\Delta_e)$ function for a parapet wall can be constructed in accordance with Equations (6b) and (6c) as shown in Figure 4(a).

Similarly, moment equilibrium can also be used to determine $F(\Delta_e)$ at the point of incipient rocking ($\Delta_e = 0^+$) for a wall simply supported at the top and bottom. By considering moment equilibrium of the upper half of a simply supported wall (of height $= h/2$ and mass $= M/2$) about the pivot point in the cracked cross-section at the mid-height of the wall leads to

$$(Mg/2)t/2 = R(h/2) - (F_0/2)(h/6) \tag{7a}$$

where R is the horizontal reaction at the top of the wall and F_0 the force F at $\Delta_e = 0^+$ (refer Figure 3(b)). R can be obtained by considering rotational equilibrium of the simply supported wall as a whole about the pivot point at the base, and is given by the following equation:

$$R = F_0/2 - Mgt/(2h) \tag{7b}$$

Substitution of Equations (7b) and (3) into Equation (7a), combined with some algebraic manipulation, leads to

$$F_0 = 4M_e(gt/h) \tag{7c}$$

For a wall simply supported along its top and bottom edges, the force F required for static equilibrium of the wall at the point of instability ($\Delta_e = 2/3t$ or alternatively $\Delta_m = t$) is

$$F = 0 \tag{7d}$$

The $F(\Delta_e)$ function for a simply supported non-loadbearing wall, as shown in Figure 4(b), can be constructed in accordance with Equations (7c) and (7d). It is also clear from Figure 4 that the general shape of the $F(\Delta_e)$ function is the same for parapet walls and walls simply supported along their top and bottom edges. The generic shape for both curves can be described by the expression

$$F = F_0(1 - \Delta_e/\Delta_{e,\max}) \tag{7e}$$

where $\Delta_{e,\max}$ is the displacement at the point of instability and F_0 the force required to initiate rocking.

Alternatively, the $F(\Delta_e)$ functions shown in Figures 4(a) and 4(b) can be defined generically in terms of the two parameters: (i) F_0 which is as defined previously, and (ii) K_0 which is the tangent stiffness of the softening slope for the wall associated with P–Δ effects. The values of F_0 for a parapet wall and a non-loadbearing simply supported wall have previously been shown (Equations (6b) and (7b)) to be $F_0 = F(\Delta_e = 0) = M_e(gt/h)$ and $F_0 = F(\Delta_e = 0) = 4M_e(gt/h)$, respectively. The tangent stiffness, K_0, is given by $K_0 = F_0/\Delta_{e,\max}$. Substitution of the expressions above for F_0 and the values for $\Delta_{e,\max}$ (shown in Figure 4) gives $K_0 = 1.5M_eg/h$ for parapet walls and $K_0 = 1.5 \times 4M_eg/h = 6M_eg/h$ for simply supported walls. Note, the factor of 1.5 arises from the definition of the effective stiffness which is defined in accordance with the effective displacement (Δ_e), as opposed to the maximum displacement at the top of the parapet wall (Δ_t) or at the mid-height of the simply supported wall (Δ_m).

The comparison of Figure 4(a) with 4(b) shows that the behaviour of URM walls possessing different support conditions can be represented by one generic model. For example, the response behaviour of a non-loadbearing simply supported wall can be simulated by a parapet wall of identical thickness and aspect ratio (h/t) which is one-quarter of the original value. Where an overburden pressure is applied (refer Figures 1(c) and 4(b)), the effect can be modelled by further reducing the aspect ratio of the equivalent parapet wall. The equivalent aspect ratio, $(h/t)_{eq}$, and equivalent thickness, t_{eq}, have been determined for walls with different boundary conditions, as shown in Table I. Clearly, the displacement capacity is largely a function of the wall thickness whereas the strength capacity is significantly influenced by the wall boundary conditions.

Table I. Equivalent aspect ratio and thickness.*

Support type	Reference	$(h/t)_{eq}/(h/t)_{actual}$	t_{eq}/t_{actual}
Rigid parapet	Figure 1(a)	1	1
Rigid non-loadbearing simply supported wall with base reaction at the leeward face	Figure 1(b)	1/4	1
Rigid loadbearing simply supported wall with top and base reactions at the leeward face	Figure 1(c)	$1/(4\{1+\Psi\})$	1
Rigid loadbearing simply supported wall with top reaction at centreline and base reaction at the leeward face	Figure 1(d)	$1/(4\{1+\Psi\})$	$(1+3/4\Psi)(1+\Psi)$ varies between 3/4 and 1

*Ψ—Ratio of overburden weight and self-weight of the upper-half of the wall above mid-height.

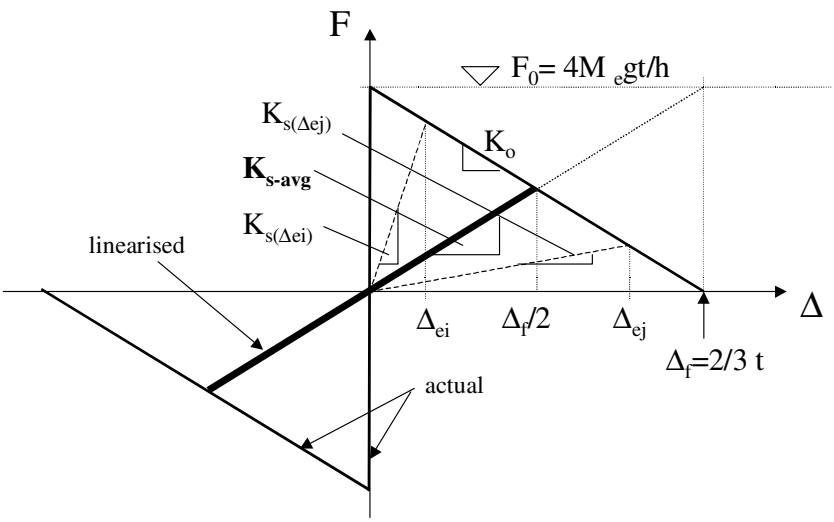

Figure 5. Average secant stiffness ($K_{s\text{-}avg}$) of rigid URM walls.

The non-linearity of the $F(\Delta_e)$ functions as shown in Figures 4(a) and 4(b) also means that URM walls do not rock with a unique natural frequency, as would be the case for a linear elastic system. In fact, the instantaneous rocking frequency is amplitude dependent, and can be approximated by considering the secant stiffness defined in accordance with the maximum displacement amplitude of the wall (Δ_e) in an average half-cycle. Such amplitude-dependent secant stiffness values, $K_{s(\Delta_e)}$, are shown in Figure 5 for the displacements at Δ_{ei} and Δ_{ej}. The secant stiffness values can be defined by the following equations:

$$K_{s(\Delta_e)} = (F_0 - K_0\Delta_e)/\Delta_e \tag{8a}$$

or alternatively,

$$K_{s(\Delta_e)} = F_0/\Delta_e - K_0 \tag{8b}$$

where Δ_e is the maximum effective displacement of the half-cycle of rocking response.

The average secant stiffness covering the entire range of displacement, from $\Delta_e = 0$ to $\Delta_e = \Delta_{e,max}$ can be defined as the secant stiffness at $\Delta_e = \Delta_{e,max}/2$ and is given by (refer Figure 5).

$$K_{s\text{-}avg} = K_0 \tag{8c}$$

This so-called 'average' secant stiffness corresponds to a line going through the centroid of the area under the non-linear force–displacement curve shown in Figure 5. The instantaneous amplitude-dependent natural frequency, $f(\Delta_e)$, and the 'average' frequency, $f_{s\text{-}avg}$ is accordingly given by the following equations, respectively:

$$f(\Delta_e) = (1/2\pi)\sqrt{(F_0/\Delta_e - K_0)/M_e} \tag{9a}$$

$$f_{s\text{-}avg} = (1/2\pi)\sqrt{K_0/M_e} \tag{9b}$$

The non-unique nature of the natural frequency resulting from the non-linearity generates problems in using an elastic response spectrum to estimate the maximum rocking response. Consequently, non-linear THA programmes have been developed by the authors to account for the effects of the non-linear force–displacement behaviour as described above and shown in Figure 4. The prediction of rocking displacement response requires a large number of accelerograms in order to obtain a reasonable prediction of the average of the ensemble. This is time-consuming, expensive and often impractical, particularly if there is an insufficient number of representative accelerograms available. Thus, alternative and simplified analytical methods have been developed.

Initially, a parametric study involving the non-linear THA of 500 Gaussian pulses, with variable pulse duration and intensity, were carried out to study the frequency-dependent response behaviour of URM walls [12, 13]. An important finding from these analyses was that the wall developed exceptionally large amplifications of displacements when the applied pulse excitations were at a particular natural (resonant) frequency. Thus, each URM wall seemed to possess a unique natural frequency, depending on the geometry of the wall and the boundary conditions, despite its non-linear properties. It was, therefore, postulated that the 'effective natural frequency' (f_{eff}), as identified from the pulse analyses, could be used with an elastic displacement response spectrum (DRS) to determine the response spectral displacement ordinates. The latter could be interpreted as the displacement demand in the URM wall during rocking. Interestingly, the observed effective natural (resonant) frequency (f_{eff}) was found to agree well with the 'average' natural frequency ($f_{s\text{-}avg}$) calculated using the secant stiffness value as given by Equations (8c) and (9b).

Finally, the viscous damping ratio (ζ) must be determined in order that the appropriate damping curve can be used in the displacement response spectrum. As for most structural systems, the critical damping ratio (ζ) of a rocking wall can be obtained experimentally by observing the rate of decay in amplitude during free-vibration. Shaking-table experiments carried out by the authors [7] in the early phase of the research programme identified the

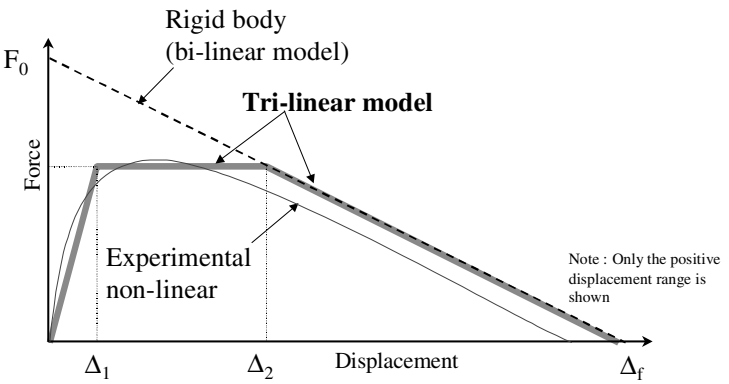

Figure 6. Force–displacement relationship of deformable URM walls.

value of ζ for parapet walls to be in the order of 3 per cent using this technique. The viscous damping factor can also be calculated from dynamic equilibrium as the net difference between the experimentally determined inertia force and the restoring force (according to the recorded acceleration and displacement, respectively) at any instant of time during the rocking response. Subsequent free-vibration experiments carried out on a range of simply supported walls [12] indicated that damping ratios were of a similar order. This critical damping ratio can be translated into a viscous damping factor using the following equation to carry out non-linear THA:

$$C = 2\zeta\omega M_e = 4\pi f \zeta M_e \tag{10}$$

where ω is the angular velocity of the linearized system. Further details considering the frequency dependence (and hence amplitude dependence) is provided in Reference [12].

4. MODELLING OF CRACKED UNREINFORCED MASONRY WALLS AS DEFORMABLE (SEMI-RIGID) BLOCKS

The bilinear force–displacement relationship described in the previous section is based on the assumption that URM walls behave essentially as rigid bodies which rock about pivot points positioned at cracks. It has been confirmed by experimental static push-over tests that the individual blocks of the URM wall can deform significantly when subjected to high pre-compression. This results in: (i) pivot points possessing finite dimensions (rather than being infinitesimally small) so that the resistance to rocking is associated with a lever arm significantly less than half the wall thickness (as for a rigid wall) and (ii) the wall possessing finite lateral stiffness (rather than being rigid) prior to incipient rocking. Importantly, the threshold resistance to rocking is reduced significantly from the original level associated with a rigid wall, to a 'force plateau' as shown in Figure 6. It can be further seen from Figure 6 that the F–Δ relationship observed during the experiment deviates significantly from this bilinear relationship and assumes a curvilinear profile. This is largely due to the non-linear

Table II. Empirically derived trilinear F–Δ defining displacements.

State of degradation at cracked joint	Δ_1/Δ_f	Δ_2/Δ_f
New	6%	28%
Moderate	13%	40%
Severe	20%	50%

deformations that occur in the mortar joint. However, there is relatively little deviation from the original bilinear model at large displacements.

This curvilinear profile can be idealized by a trilinear model that is defined by three displacement parameters: $\Delta_{e,1}$, $\Delta_{e,2}$ and $\Delta_{e,max}$ and the force parameter F_0 (refer Figure 6). To construct the trilinear model, the bilinear model is first constructed in accordance with F_0 and K_0. The amplitude of the force plateau is, therefore, controlled by the ratio Δ_2/Δ_f. For displacements in the range exceeding Δ_2, the trilinear and the bilinear models coincide. For displacements between Δ_1 and Δ_2, the force is constant. The initial slope of the trilinear model is governed by the force amplitude of the plateau and the value of Δ_1.

The ratios Δ_1/Δ_f and Δ_2/Δ_f are related to the material properties and the state of degradation of the mortar joints at the pivot points. Data recorded during many quasi-static and dynamic tests of 14 simply supported walls suggests nominal values for the ratios of Δ_1/Δ_f and Δ_2/Δ_f for walls in 'new', 'moderately degraded' and 'severely degraded' condition as shown in Table II. The interpretation of the 'moderately degraded' and 'severely degraded' conditions are highly subjective. From the experimental tests, the effective width of the mortar in the cracked bedjoint for walls classified as severely degraded was approximately 90 per cent of the original width. Moderately degraded walls had effective bedjoint widths that were essentially equal to their original widths. However, the exposed vertical faces of the mortar joints had rounded due to some rocking having taken place. Full details of these tests are given in Reference [13]. This trilinear F–Δ relationship proved to be effective for the walls tested in this study over the full range of degradation.

The traditional method of selecting a secant stiffness for use with a substitute structure representation of a multi-degree-of-freedom system is not straightforward for non-ductile systems such as URM. One method commonly used is to adopt the secant stiffness from the system's non-linear force–displacement curve corresponding to the point of maximum (permissible) displacement. For ductile systems, this is often associated with a point on the post-peak softening section of the non-linear force–displacement curve where the force has reduced to some fraction (75–80 per cent is common) of the peak force value. In this study, and for masonry in general, it was not simple to define this point due to material strength variability and a lack of definitive yield and/or softening points. However, it was observed that the stiffness corresponding to a line going through the point on the trilinear force–displacement curve where $\Delta = \Delta_2$ as shown in Figure 7 was reasonably consistent with this notion.

The effective secant stiffness, $K_{s\text{-eff}}$, for the semi-rigid wall obtained in this manner can be expressed mathematically in generic terms as

$$K_{s\text{-eff}} = K_0 \left(1 - \frac{1}{\Delta_2/\Delta_1}\right) \tag{11}$$

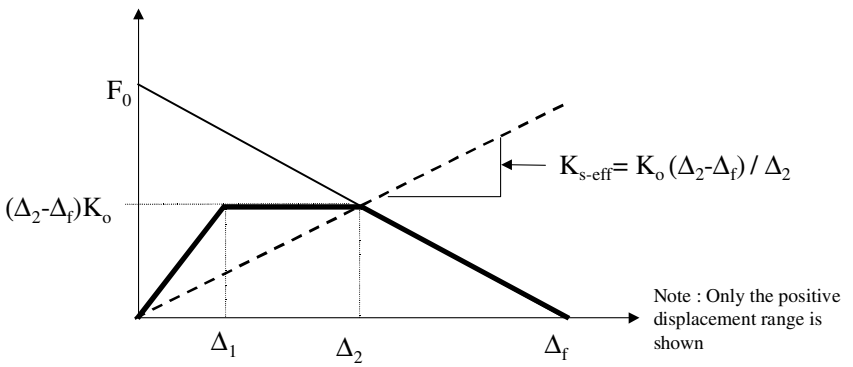

Figure 7. Effective secant stiffness ($K_{\text{s-eff}}$) of semi-rigid walls.

where K_0 is defined as shown in Figures 5 and 6 and values for Δ_2/Δ_1 are given by Table II. The effective undamped natural frequency, $f_{\text{s-eff}}$, for the equivalent SDOF system is accordingly given by the following equation:

$$f_{\text{s-eff}} = \frac{\sqrt{K_{\text{s-avg}}/M_{\text{e}}}}{2\pi} \tag{12}$$

The experimentally observed 'resonance' frequency for each of the test walls was found to agree well with estimates given by Equation (12) using effective secant stiffness values as defined above. (Note: using the approach of Section 3 where the effective stiffness was taken as the slope of the line going through the centroid of the area under the force–displacement curve gives similar results.)

5. DISPLACEMENT DEMAND PREDICTION BY SUBSTITUTE STRUCTURE IDEALIZATION

The DB analysis methodology provides a rational means for determining seismic design actions as an alternative to the more traditional 'quasi-static' force-based approach. In the DB method, the dynamic lateral displacement capacity of a structure, subjected to an excitation is determined based on a comparison of the displacement demand imposed on the structure during a seismic event with a pre-determined critical displacement capacity. The 'substitute structure' methodology proposed by Shibata and Sozen [14] was adopted to simplify highly non-linear systems into a linearized DB procedure. An elastic SDOF oscillator is selected with linear properties that characterize those of the real non-linear structure. The effectiveness of the linearized DB procedure is reliant on the assumption that both the 'substitute structure' and real system will reach the same critical displacement under the same excitation.

It was observed from the parametric studies using Guassian Pulses (described in Section 3) that incipient instability most likely occurs as a consequence of the large displacement amplifications associated with resonance of the wall. The effective resonant frequency, f_{eff}, is related to a particular effective secant stiffness. It appears that the displacement demand of URM walls arising from rocking can be predicted using the linearized DB analysis procedure

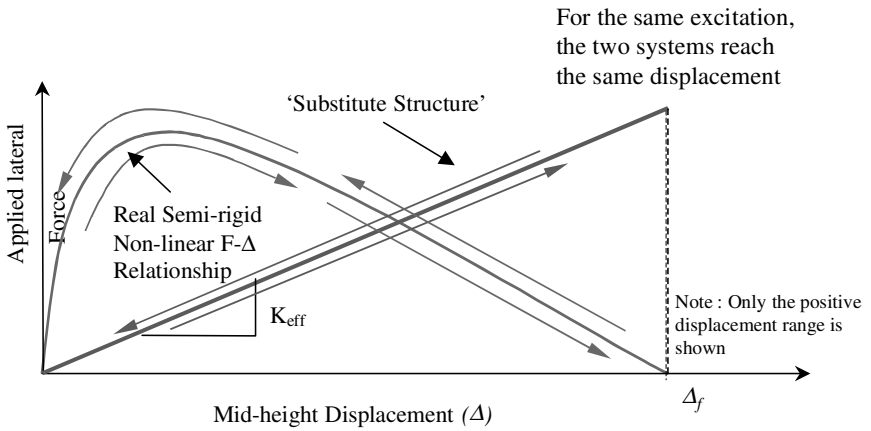

Figure 8. Characteristic linear 'substitute structure' stiffness (K_{eff}) for displacement analysis.

Table III. Earthquake records used in study.

Earthquake	PGA
El Centro, 18 May 1940, S00E component	0.35*g*
Taft, 21 July 1952, S69E component	0.18*g*
Pacoima Dam, 9 February 1971, S14W component	1.08*g*
Nahinni (aftershock), 23rd December 1985	0.23*g*

provided that a suitable 'substitute structure' effective secant stiffness has been selected (refer Figure 8). As noted in Section 3, the values of K_{eff} obtained from the Gaussian pulse study were found to be consistent with the values for $K_{\text{s-eff}}$ defined by Equation (11). The consistency of this finding was confirmed by comparing the results of non-linear THA and shaking table experiments.

An extensive analytical study was conducted to test the effectiveness of the linearized DB procedure for face loaded simply supported URM walls. The non-linear THA software ROMANRY (which has been further developed from the original program, ROMAIN, reported in Reference [15]), formed the basis of the study. The accuracy of the THA procedure was verified using results of shake table tests as described in Reference [12]. Representative wall configurations which included various aspect ratios, overburden stresses and degrees of joint degradation were selected for examination. Only the boundary conditions shown in Figures 1(b) and 1(c) (refer also to Table I) were considered in the study. The benefit of vertical edge wall constraints (e.g. reinforced concrete columns) and possible arching action as might occur in URM infill walls in a concrete frame [9] were not considered in this paper.

5.1. Examples using the displacement-based analysis method

The verification analyses used scaled accelerograms of four real earthquake records (listed in Table III) including the well-known El Centro record. Initially, a 3.3m tall, 110mm thick wall

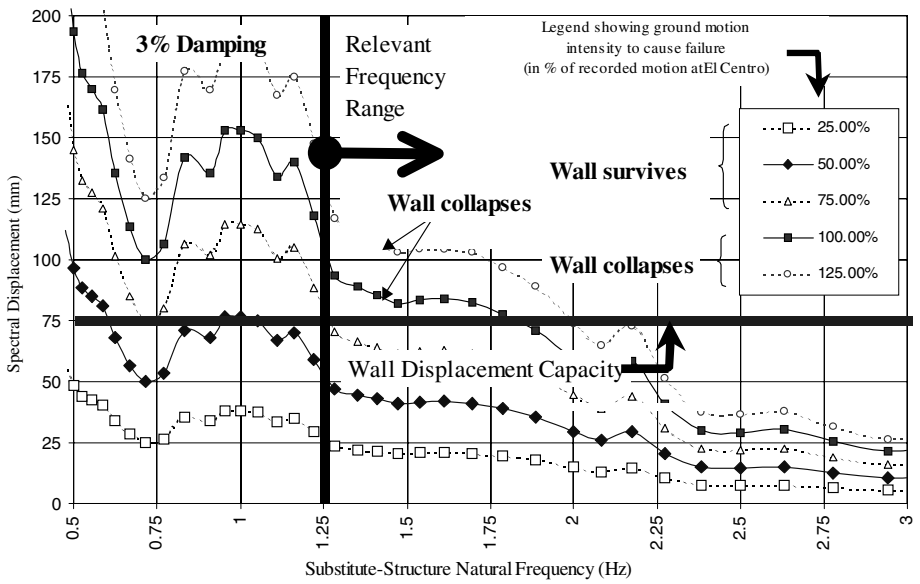

Figure 9. Displacement-based assessment of URM wall for El Centro motion.

with 0.075MPa applied overburden stress and moderately degraded rotation joints was analyzed using the normalized El Centro acceleration record. Figure 9 presents the elastic displacement response spectra (3 per cent damping) for the El Centro record scaled by percentages in the range from 25 per cent to 125 per cent, in 25 per cent increments. The horizontal line at 73 mm ($= 2/3 \times 110$ mm) represents the displacement capacity of the 'substitute structure', Δ_f. The natural frequency of the substitute structure, f_{eff}, as determined from $K_{\text{s-eff}}$, was 1.23 Hz. It must be recognized that the rocking frequency which occurs during a response is displacement dependent, i.e. the frequency varies from a large value associated with an uncracked elastic response to the effective frequency as defined in Equation (12). Thus, only frequencies greater than $f_{\text{s-eff}}$ were considered in the analyses. Using this criterion, the lowest scaled El Centro earthquake from all frequencies greater than f_{eff} to cause instability of the wall was 70 per cent, as shown in Figure 9. The instability resistance of this wall when subjected to a normalized El Centro record is therefore (70 per cent $\times$ 0.35g) 0.24g as assessed using the proposed DB assessment methodology. For comparison the instability resistance prediction using non-linear THA was 0.28g thus indicating good correlation between the DB and THA methods.

Using the traditional 'quasi-static' force-based (FB) prediction (refer Equation (7c) and Table I) the assessed instability resistance is 0.29g based on the strength of the 'moderately degraded' wall which is approx. 60 per cent of the strength of a 'perfectly rigid' wall (refer Figure 6 and Table II). Thus, the DB, THA and FB methods provide similar instability predictions for the wall when subject to the El Centro excitation. Importantly, this is not the case should the predominant frequency of the record used be characterized by a high acceleration but low displacement demand such as the Nahanni excitation. When the same

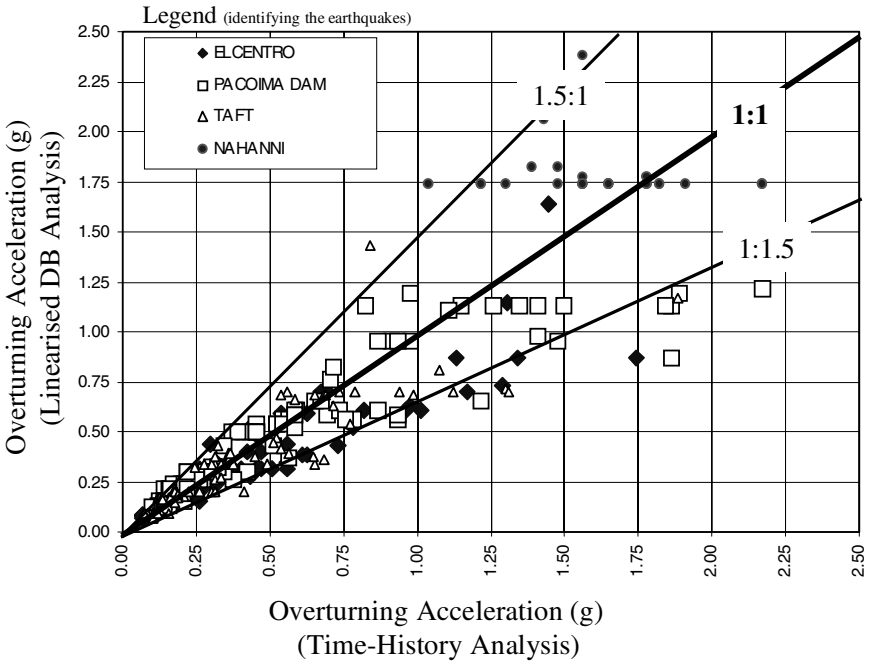

Figure 10. Accuracy evaluation of 'linearized DB' analysis.

wall is subject to the Nahanni excitation, the instability prediction obtained from the DB and the THA method is 1.8g and 1.4g, respectively. Again, the results obtained from the two methods are in reasonable agreement but are significantly different to 0.29g obtained from the FB method. These two examples show that the response behaviour of the wall is highly dependent on the frequency characteristics of the excitation. Such effects are not fully accounted for by the conventional FB calculations which neglect the significant reserve capacity of the wall to undergo large displacements (through rocking) without overturning.

5.2. Parametric study results

The linearized DB procedure was then repeated using the four different earthquake records (refer Table III) for various height, thickness and applied overburden wall configurations. The respective earthquake scaling factors corresponding to failure ($\Delta_e = \Delta_f$) were compared with the predictions from the non-linear THA as shown in Figure 10. It can be observed that nearly all the results are located within the $\pm 50\%$ certainty bounds indicating that regardless of the characteristics of the excitation the linearized DB procedure provides reasonable estimates of instability resistance. The scatter in the results is due primarily to the linearization of the non-linear rocking wall system.

The scatter in results could be accounted for in the DB assessment of URM walls by using an uncertainty factor of 1.5 as follows. For the 110 mm thick wall considered in the previous example ($\Delta_f = 0.67t = 73$ mm), its capacity to resist excitations would be calculated to be

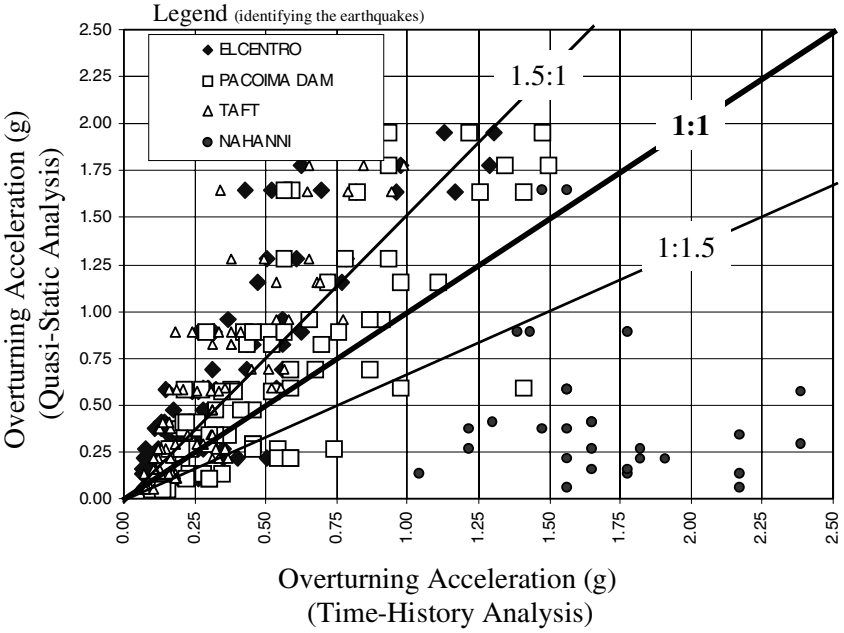

Figure 11. Accuracy evaluation of 'quasi-static' analysis.

50 mm (i.e. $(\frac{2}{3})110/1.5$) at the wall boundaries. Many intraplate earthquakes observed in the past on rock and stiff soil sites had their spectral displacements well within this 50 mm limit even though their peak ground accelerations could well exceed the stability limit according to FB calculations ($0.29g$ from the above example). Some examples of these recorded excitations are shown and analysed in Lam *et al.* [16, 17]. Thus, DB calculation is generally more realistic than FB calculations when analysing high-frequency excitations. On the other hand, the DB method also identifies walls located on soft soil sites and/or at the upper levels of a building to be particularly vulnerable due to the amplified low-frequency excitations which can be translated into high displacement thus causing overturning.

Nevertheless, while the scatter observed in Figure 10 is not insignificant, it is much less than that observed for the corresponding set of force-based analyses. A comparison of the 'quasi-static' rigid body predictions with THA predictions is presented in Figure 11 which clearly shows a much wider scatter compared with the linearized DB analysis. This additional scatter is largely due to the dependence of the accuracy of the 'quasi-static' rigid body predictions to the characteristics of the excitation as well as the difference in theoretical rigid resistance and the real semi-rigid resistance approximated by the plateau of the trilinear force–displacement relationship. In particular, the seismic resistant capacity of the URM walls is significantly underestimated for the higher frequency Nahanni earthquake (which is characterized by a high acceleration but low-displacement demand) if the 'reserve capacity' associated with rocking is ignored.

6. SUMMARY AND CONCLUSIONS

A simplified linearized displacement-based (DB) procedure has been presented together with recommendations for the selection of an appropriate 'substitute structure' in order to provide the most representative analytical results. A trilinear relationship was used to characterize the real non-linear force–displacement relationship for unreinforced brick masonry walls (Figure 6). The effective secant stiffness for the 'substitute structure' corresponding to the line going through the $\Delta = \Delta_2$ point on the trilinear force–displacement curve (Figure 7) was found to correlate well with the predominant natural frequencies observed during experimental testing.

Predictions from the linearized DB analysis and the 'quasi-static' analysis procedures have been compared with the non-linear THA results. The respective scatter for the DB and force-based procedures was seen to be much less for the linearized DB analysis procedure. In particular, the DB procedure was seen to be substantially better for earthquake ground motions with high accelerations and low displacements such as might be expected for ground motions in low to moderate seismicity regions. In short, while the current DB procedure as described in this paper has some shortcomings, it appears to be an improvement over the current force-based procedure. Further work is still required (i) to refine the method and (ii) to investigate the implications of using linearized methods to represent non-linear behaviour in a substitute structure procedure.

REFERENCES

1. Calvi GM, Kingsley GR. Displacement-based seismic design of multi-degree-of-freedom bridge structures. *Earthquake Engineering and Structural Dynamics* 1995; **24**(9):1247–1266.
2. Moehle JP. Displacement based seismic design criteria. *Proceedings of the 11th World Conference on Earthquake Engineering*. Elsevier Science Ltd.: Pergamon, 1996; Disc 4, Paper No. 2125.
3. Priestley MJN. Displacement-based seismic assessment of reinforced concrete buildings. *Journal of Earthquake Engineering* 1997; **1**(1):157–192.
4. Bruneau M. State of the art report on seismic performance of unreinforced masonry buildings. *ASCE Journal of Structural Engineering* 1994; **120**(1):230–251.
5. ABK. Methodology for the mitigation of seismic hazards in existing unreinforced masonry buildings: the methodology. *ABK Topical Report 08*, El Segundo, California, 1984.
6. Bariola J, Ginocchio JF, Quinn D. Out of plane seismic response of brick walls. *Proceedings of the 5th North American Masonry Conference*, 1990; 429–439.
7. Lam N, Wilson J, Hutchinson G. The seismic resistance of unreinforced masonry cantilever walls in low seismicity areas. *Bulletin of The New Zealand National Society of Earthquake Engineering* 1995; **28**(3):79–195.
8. la Mendola L, Papia M, Zingone G. Stability of masonry walls subjected to seismic transverse forces. *ASCE Journal of Structural Engineering* 1995; **121**(11):1581–1587.
9. Abrams DP, Angel R, Uzarski J. Out-of-plane strength of unreinforced masonry infill panels. *Earthquake Spectra* 1996; **12**(4):825–844.
10. Priestley MJN. Seismic behaviour of unreinforced masonry walls. *Bulletin of the New Zealand National Society for Earthquake Engineering* 1985; **18**(2):191–205.
11. Tena-Colunga A, Abrams DP. Seismic behavior of structures with flexible diaphragms. *ASCE Journal of Structural Engineering* 1996; **122**(4):439–445.
12. Doherty K, Lam N, Griffith M, Wilson J. The modelling of earthquake induced collapse of unreinforced masonry walls combining force and displacement principals. *Proceedings of the 12th World Conference on Earthquake Engineering*, Auckland, New Zealand, 2000; Paper 1645.
13. Doherty K. An investigation of the weak links in the seismic load path of unreinforced masonry buildings. *PhD Thesis*, Adelaide University, Department of Civil and Environmental Engineering, 2000.
14. Shibata A, Sozen MA. Substitute-structure method for seismic design in R/C. *Journal of the Structural Division, Proceedings of the American Society of Civil Engineers*, 1976; **102**, No. ST1.

15. Lam NTK, Wilson JL, Hutchinson GL. Time-history analysis for rocking of rigid objects subjected to base-excitations. *Proceedings of the 14th ACMSM*, vol. 1, Hobart, 1995; 284–289.
16. Lam NTK, Wilson JL, Hutchinson GL. Generation of synthetic earthquake accelerograms using seismological modelling: a review. *Journal of Earthquake Engineering* 2000; **4**(3):321–354.
17. Lam NTK, Wilson JL, Chandler AM, Hutchinson GL. Response spectrum modelling for rock sites in low and moderate seismicity regions combining velocity, displacement and acceleration predictions. *Earthquake Engineering and Structural Dynamics* 2000; **29**(10):1491–1526.

